

Uniform Field in Microwave Cavities Through the Use of Effective Magnetic Walls

Jim A. Enriquez,^{1, a)} Rustam Balafendiev,^{2, a)} Alexander J. Millar,^{3,4} Constantin Simovski,⁵ and Pavel Belov^{6,7}

¹⁾ *Physics Department, National University of Colombia, 111321, Bogota, Colombia*

²⁾ *Science Institute, University of Iceland, Dunhagi 5, 107 Reykjavik, Iceland*

³⁾ *Theoretical Physics Division, Fermi National Accelerator Laboratory, Batavia, IL 60510, USA*

⁴⁾ *Superconducting Quantum Materials and Systems Center (SQMS), Fermi National Accelerator Laboratory, Batavia, IL 60510, USA*

⁵⁾ *Department of Electronics and Nanoengineering, Aalto University, Maarintie 8, FI00076, Espoo, Finland*

⁶⁾ *Qingdao Innovation and Development Center, Harbin Engineering University, Qingdao 266000, Shandong, China*

⁷⁾ *School of Engineering, New Uzbekistan University, Movarounnahr str. 1, 100000, Tashkent, Uzbekistan*

(Dated: 28 November 2024)

Wire media (WM) resonators have emerged as promising realization for plasma haloscopes – devices designed to detect axions, a potential component of dark matter. Key factors influencing the detection probability include cavity volume, resonance quality factor, and form factor. While the form factor has been explored for resonant frequency tuning, its optimization for axion detection remains unexplored. In this work, we present a novel approach to significantly enhance the form factor of WM plasma haloscopes. By shifting the metal walls of the resonator by a quarter wavelength, we effectively convert an electric wall boundary condition into a magnetic wall one, allowing for an almost uniform mode. Theoretical analysis and numerical simulations confirm that this modification improves the electric field profile and boosts the form factor. We validate these findings through experimental results from two prototype resonators: one with a standard geometry and another with a quarter-wave air gap between the WM and the walls. Additionally, our method provides a simple way to control the field profile within WM cavities, which can be explored for further applications.

Wire media (WM), introduced by Brown¹ and Rotman² and later advanced by Pendry and Belov et al.^{3,4}, are artificial plasma materials with tunable plasma frequencies determined by their geometric parameters. These dense arrays of metallic wires embedded in a dielectric host have been applied in diverse fields, ranging from microwave antennas⁵ to near-field thermophotovoltaic systems⁶, and systems of radiative cooling⁷ (see Ref. 8 for a detailed review).

Research on WM open resonators has primarily focused on utilizing topological transitions in isofrequency contours to enhance the Purcell factor^{9,10}. Recently, WM cavities enclosed by metallic walls and placed in a DC magnetic field—known as plasma haloscopes¹¹—have emerged as a promising technique for detecting axions, a dark matter candidate¹². These cavities can also be used to search for dark photons, another dark matter candidate, even in the absence of a magnetic field¹³. Our previous work demonstrated that WM operating in the epsilon-near-zero (ENZ) regime significantly extends the wavelength of light, achieving low-frequency resonance and high field uniformity¹⁴.

Field homogeneity in microwave resonators has been studied in the context of electron paramagnetic resonance (EPR), where axially uniform TE modes are desirable¹⁵.

A common method involves a central metallic waveguide operating at its cutoff frequency, flanked by end regions with optical lengths set to a quarter wavelength¹⁵. Proposed configurations for the end regions include dielectric rods matching the central cross-section¹⁶, enlarged cross-sections¹⁷, and conducting rod insertions¹⁸.

For axion haloscopes, field uniformity is as beneficial as it is for EPR devices. Key characteristics that enhance performance include the strength of the DC magnetic field, cavity volume, quality factor, and form factor, all of which influence the power from photon-axion conversion in resonance¹⁹. The form factor for a mode in a plasma haloscope, characterized by an electric field \mathbf{E}_{lmn} , is defined as

$$C_{lmn} = \frac{|\iint_V \mathbf{B}_0 \cdot \mathbf{E}_{lmn} dV|^2}{V B_0^2 \iint_V \epsilon |\mathbf{E}_{lmn}|^2 dV}, \quad (1)$$

where V is the cavity volume, ϵ is the relative permittivity within the cavity, and \mathbf{B}_0 is the external DC magnetic field, assumed spatially constant and aligned with the wires.

To achieve optimal field homogeneity and form factor in plasma haloscopes, researchers have focused on the fundamental TM cavity mode^{20–23}. In WM resonators, the fundamental TM mode produces a uniform axial field and a sinusoidal transverse pattern due to electric wall boundary conditions and axial polarization¹⁴. Wedge-shaped haloscopes use quarter-wavelength corrugations

^{a)}These authors contributed equally.

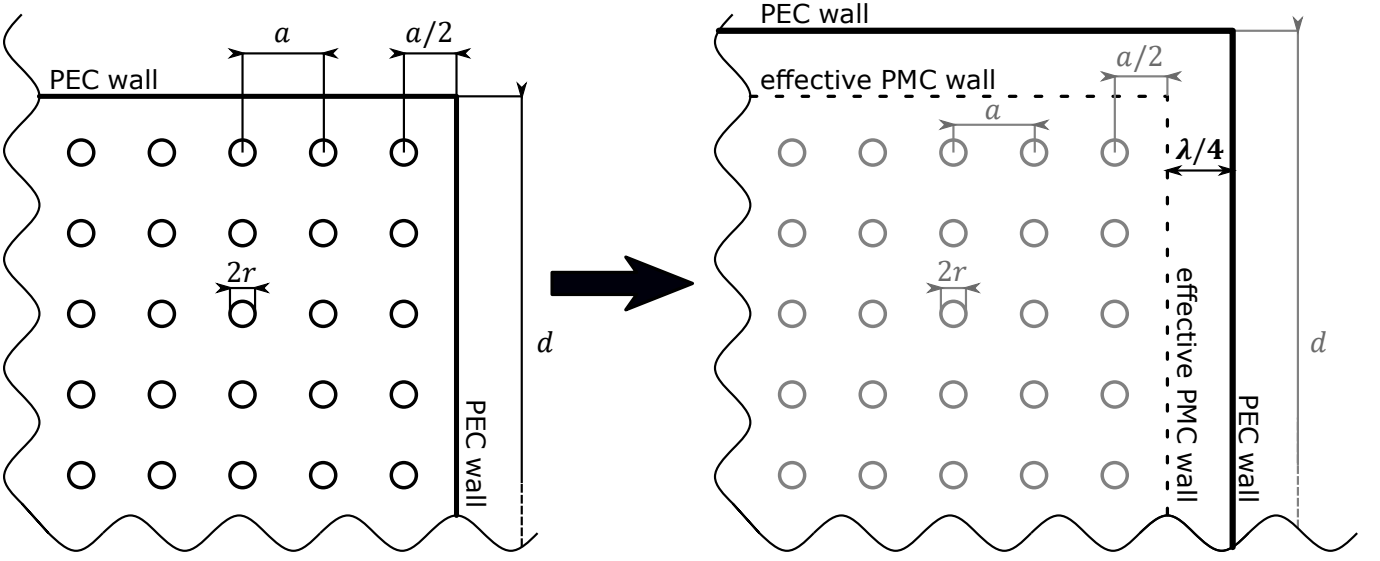


FIG. 1: Schematic of the proposed modification to the cavity's boundary condition. The WM resonator consists of metallic wires with radius r and period a . In the regular configuration, the distance between the outermost wires and the PEC walls is $a/2$. Adjusting this distance to $a/2 + \lambda/4$ transforms the boundary, making it behave as an effective perfect magnetic conductor wall.

in the walls to achieve axial field uniformity^{24,25}. However, researchers have yet to explore improving field homogeneity in the transverse direction of WM resonators.

In this work we demonstrate that placing the cavity walls with a quarter-wavelength gap from the WM interface transforms the interface from a perfect electric conductor to a perfect magnetic conductor. Figure 1 illustrates this concept. This transformation is similar to converting a shortened transmission line into an open one by shifting the termination by an odd number of quarter-wavelengths. By modifying the boundary conditions, we create a cavity with a TM_{000} mode instead of the regular TM_{110} mode, significantly improving the form factor and lowering the fundamental resonance frequency to the plasma frequency.

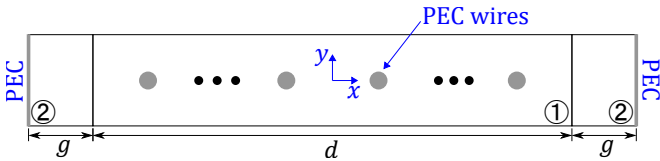


FIG. 2: One-dimensional schematic of a resonator consisting of a wire medium (region 1) with thickness d , enclosed by an air gap (region 2) of thickness g .

To evaluate the impact of this air gap on modal field uniformity, we develop a one-dimensional analytical model that focuses on TM modes, which interact most strongly with the WM. We model the system as two regions, as shown in Fig. 2. Region 1 contains the lossless WM (PEC wires) characterized by a relative permittivity⁸

$$\epsilon = 1 - \left(\frac{k_p}{k_0}\right)^2, \quad (2)$$

where k_0 is the vacuum wave number and $k_p = \frac{2\pi}{\lambda_p}$, with λ_p being the plasma wavelength. Region 2 represents the air gap between the WM and the PEC walls. Horizontal lines in Fig. 2 outline a unit cell of the infinitely extended parallel-plate cavity. By imposing the inherent odd symmetry of the electric field and even symmetry of the magnetic field due to the PECs, we derive the TM mode solutions to Maxwell's equations as follows:

$$E_z(x) = \begin{cases} A \cos(k_{x1}x) & |x| \leq \frac{d}{2} \\ B \sin(k_{x2}(\frac{d}{2} + g - |x|)) & |x| > \frac{d}{2} \end{cases}, \quad (3)$$

$$H_y(x) = \begin{cases} -jA \frac{k_{x1}}{\eta_0 k_0} \sin(k_{x1}x) & |x| \leq \frac{d}{2} \\ -j \frac{x}{|x|} B \frac{k_{x2}}{\eta_0 k_0} \cos(k_{x2}(\frac{d}{2} + g - |x|)) & |x| > \frac{d}{2} \end{cases}, \quad (4)$$

where $k_{x1} = \sqrt{\epsilon}k_0$, and $k_{x2} = k_0$, assuming no field dependence on x and z .

We derive the surface impedance for the WM-air interface by evaluating the field solutions from Eqs. (3) and (4) at $x = \frac{d}{2}^+$, just outside the WM region, yielding the following expression:

$$Z = \frac{|E_z|(\frac{d}{2}^+)}{|H_y|(\frac{d}{2}^+)} = \frac{\eta_0 k_0 \sin(k_{x2}g)}{k_{x2} \cos(k_{x2}g)}. \quad (5)$$

This impedance vanishes for $g = 0$, corresponding to a perfect electric conductor, and approaches infinity as g

tends to $\lambda/4$, matching the wave impedance of a perfect magnetic conductor.

Building on the derived surface impedance, we now investigate the TM modes of a 2D WM resonator using the 1D model. Assuming no field variation along the z -axis for the fundamental mode ($k_z = 0$) and a square resonator cross-section ($k_x = k_y = k_{t1}$), the electromagnetic field within the effective WM is given by

$$\left. \begin{aligned} E_z &= E_0 \cos(k_{t1}x) \cos(k_{t1}y) \\ H_x &= jE_0 \frac{k_{t1}}{\eta_0 k_0} \cos(k_{t1}x) \sin(k_{t1}y) \\ H_y &= -jE_0 \frac{k_{t1}}{\eta_0 k_0} \sin(k_{t1}x) \cos(k_{t1}y) \end{aligned} \right\} |x|, |y| \leq \frac{d}{2}. \quad (6)$$

In the effective WM region, defined by $|x|, |y| \leq \frac{d}{2}$, we define the wave number as

$$\epsilon k_0^2 = k_x^2 + k_y^2 = 2k_{t1}^2, \quad (7)$$

while in the air gap region, for instance where $x > \frac{d}{2}, |y| \leq \frac{d}{2}$, we define the wave number as

$$k_0^2 = k_{x1}^2 + k_{y2}^2 = k_{t1}^2 + k_{t2}^2. \quad (8)$$

Utilizing Eqs. (7) and (8), and solving for k_{t1} and k_{t2} , we obtain:

$$\begin{aligned} k_{t1}^2 &= \frac{\epsilon}{2} k_0^2, \\ k_{t2}^2 &= \left(1 - \frac{\epsilon}{2}\right) k_0^2. \end{aligned} \quad (9)$$

This model assumes the WM resonator has no corners, which may differ from a real resonator. However, we can use the one-dimensional solution to estimate the two-dimensional behavior, similar to Marcatili's method for dielectric rectangular waveguides²⁶. This approximation holds when the field is mainly concentrated in the central region.

Matching the surface wave impedance of the field at the effective WM boundary (Eqs. (6)) with that of the effective boundary condition (Eq. (5)), particularly at $x = \frac{d}{2}, |y| \leq \frac{d}{2}$, we derive the following dispersion equation:

$$k_{t1} \tan(k_{t1} \frac{d}{2}) - k_{t2} \cot(k_{t2}g) = 0. \quad (10)$$

This equation gives the resonance frequencies of the TM modes. Notably, using Eq. (9), we can determine the resonance frequency of the fundamental TM mode. For the fundamental mode, when $g = \lambda/4$, the second term in Eq. (10) vanishes, implying that $k_{t1} = 0$. Consequently, $\epsilon = 0$ and $k_0 = k_p$, leading to a constant electric field according to Eq. (6).

It is worth mentioning that Eq. (10) resembles the dispersion equation derived in Ref. 16. However, while Ref. 16 achieves field homogeneity in only one direction using a central metallic waveguide, our approach offers the advantage of ensuring field homogeneity in both

transverse directions by utilizing a WM in the central region of the cavity.

In order to quantify the field uniformity in the WM resonator, we use a 2D version of the form factor in Eq. (1),

$$C = \frac{(\iint_S E_z dS)^2}{S \iint_S |\mathbf{E}|^2 dS}, \quad (11)$$

where S is the area of the transversal section of the 2D WM resonator, $(d + 2g) \times (d + 2g)$.

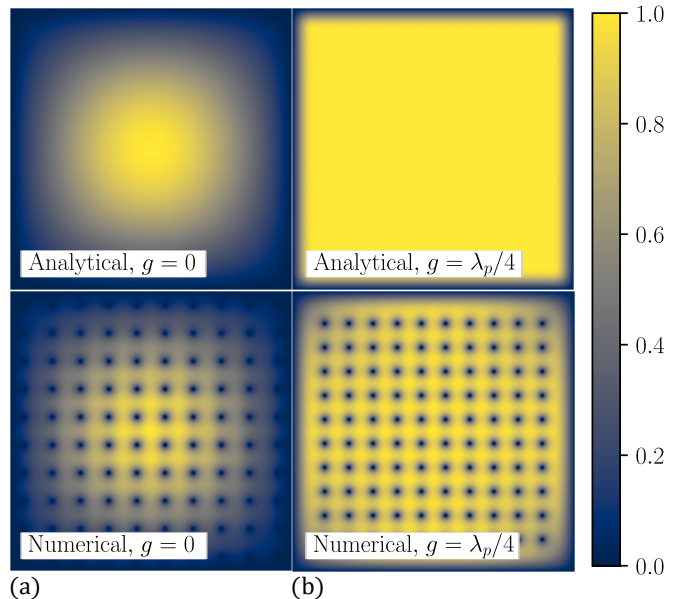


FIG. 3: Electric field distribution in a WM resonator: (a) Regular configuration with no air gap ($g = 0$) and (b) configuration with an air gap of $g = \lambda_p/4$. Introducing the air gap improves the uniformity of the electric field distribution.

We validated the applicability of our theoretical model using wave simulations with the COMSOL Multiphysics eigenmode solver. Both our analytical calculations and simulations modeled the cavity as an array of 10×10 infinitely long wires, with a wire radius of $r_0 = 0.5$ mm and inter-wire spacing $a = 10$ mm. To determine the required plasma frequency for the theoretical model, we applied a generalized quasi-static approach²⁷.

Figure 3 shows the normalized electric field distribution for the fundamental TM mode over the transverse (xy) plane of the cavity for two cases: $g = 0$ and $g = \lambda_p/4$. Both our numerical and analytical results confirm that introducing a $\lambda_p/4$ air gap homogenizes the electric field distribution in a finite-cross section sample of the WM.

The electric field profile along the x -axis for the fundamental TM mode of a WM resonator varies with the gap width, g , as shown in Fig. 4. The field homogeneity improves as g increases, reaching a maximum at $g = \lambda_p/4$. Introducing a quarter-wavelength air gap between the effective wire medium and the PEC walls significantly flat-

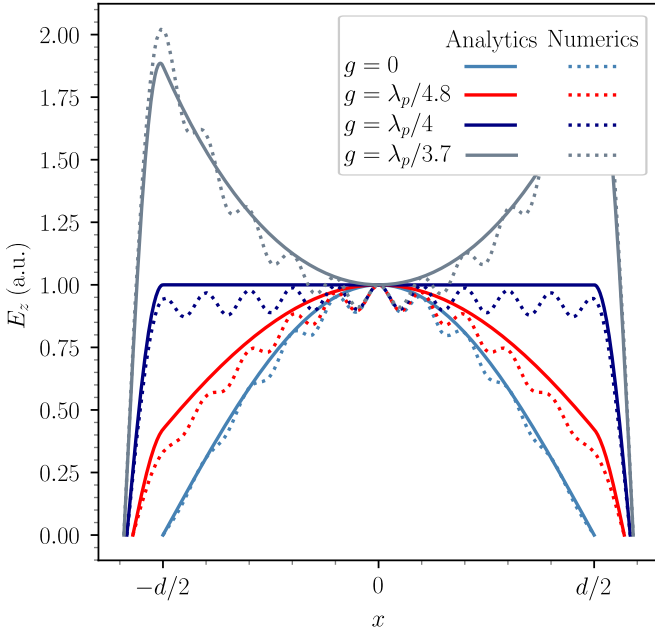


FIG. 4: WM resonator electric field profile for different air gap thicknesses, g . The WM extends from $x = -\frac{d}{2}$ to $x = \frac{d}{2}$. A uniform electric field within the WM region is achieved at $g = \lambda_p/4$.

tens the electric field profile, confining the field decay primarily to the newly added $\lambda_p/4$ region. This coincides with a pronounced magnetic field enhancement within the same gap, offering potential for readout applications. When the gap exceeds $\lambda_p/4$, the field concentrates near the resonator walls, and the underlying assumption of field confinement within the wire medium becomes not adequate.

Figure 5 illustrates the resonant frequency (Fig. 5a) and form factor (Fig. 5b) of the fundamental mode in such WM resonator as a function of the air gap, g . The resonant frequency remains nearly constant for $0 \leq g \leq \lambda_p/4$, aligning with the plasma frequency at $g = \lambda_p/4$. Conversely, the form factor progressively increases, reaching a maximum at an air gap of approximately $g = \lambda_p/4$. While the resonant frequency exhibits excellent agreement between analytical and numerical results, coming from both a physical WM and an effective WM, within this range, a slight discrepancy arises in the form factor. This error results from the evident difference between the effective and physical (real) WM. In the effective-medium model there are no wires and the field does not vanish inside this medium, whereas in the physical WM it vanishes within every wire – see the dark spots in the bottom panel of Fig. 3b.

Numerical calculations of the mode field for an effective WM show a maximum form factor of 0.92 at 8.9 GHz with $g = \lambda_p/4 = 8.4$ mm, consistent with the analytical model. However, the simulation of the physical WM corresponding to the bottom panel of Fig. 3b shows the form factor 0.89. Despite this, both numerical

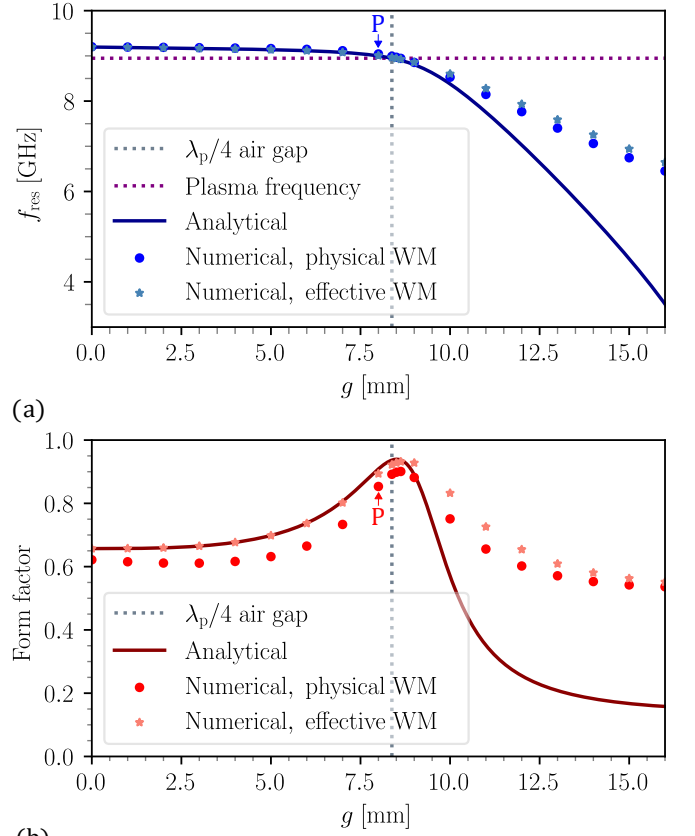


FIG. 5: Characteristics of the fundamental TM mode in a WM resonator: (a) Resonance frequency and (b) form factor as functions of air gap thickness, g . At $g = \lambda_p/4$, a form factor of approximately 0.92 is achieved for the effective WM (theory and simulations), while a value of 0.89 is observed for the physical WM (simulations).

Point P indicates the air gap thickness applied in the experimental setup.

and analytical results agree on the air gap value for the maximum form factor. For smaller gaps the agreement between the analytical and numerical results corresponding to the physical WM is good, and is excellent for the numerical simulations of the effective WM sample surrounded by the PEC walls. Thus, these results fully justify the model of an effective WM sample for $g \leq \lambda_p/4$. For $g > \lambda_p/4$, the analytical model diverges from numerical simulations due to field concentration in the air gap, which invalidates the assumption of field confinement within the WM. Nonetheless, numerical results for the effective WM and the array of separate wires remain consistent.

The maximal form factor corresponds to the perfect magnetic wall effectively located at the WM-air interface. The PEC wall shifts the phase of a reflected wave by π , the air gap grants an extra π , so the phase of the reflected wave does not change. Therefore, the mode inside the WM sample is the standing wave shaped by four per-

fect magnetic boundaries surrounding the sample. Note that this effective boundary condition can be achieved through various methods that introduce an extra phase shift of π between incident and reflected waves, as detailed in^{16–18}. This flexibility may facilitate the implementation of TM_{000} modes in tunable plasma haloscope designs.

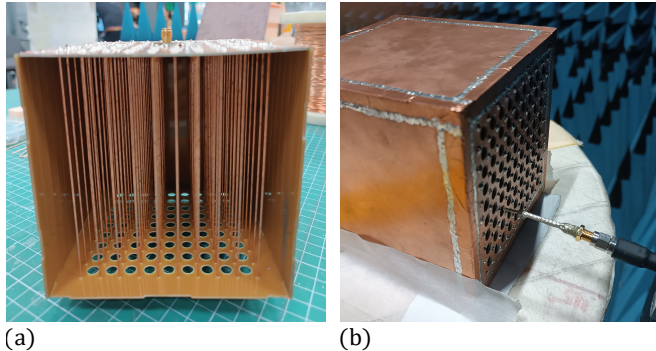


FIG. 6: Prototype WM resonators with different wall spacings, consisting of 10×10 arrays of copper wires with a period of $a = 1$ cm. The first resonator is regular with a distance of $a/2$ between the edge wires and the walls, and the second is $\lambda/4.2$ -shifted, with spacing $a/2 + \lambda/4.2$. (a) Unfinished state of the regular resonator with copper wires (radius 0.5 mm) inserted into the FR-4 PCB walls. (b) Finished prototype being scanned through pre-drilled holes by a movable antenna.

To validate the claimed effect, we fabricated two prototypes. The first prototype represents the regular (conventional) configuration where the air gap between the array of wires and the cavity walls is $a/2$ ¹⁴. The second prototype incorporates a configuration we specially optimized for the cubic resonator to enhance field homogeneity and to avoid situations where the air gap exceeds $\lambda_p/4$, as this would lead the field to localize mainly near the cavity walls (see Fig. 4). In this 3D case, the designed gap is slightly smaller than the quarter-wavelength. So, for the optimized resonator, the edge wires of the array are distanced from the walls by $(a/2 + \lambda_p/4.2)$. For the 2D resonator, this configuration would correspond to point P in Fig. 5. Below we call our optimized cubic resonator the $\lambda_p/4.2$ -shifted one.

We fabricated the prototype enclosures using single-sided metal FR-4 PCBs of 1 mm thickness. We arranged these PCBs into cubes with dimensions of 10 cm x 10 cm x 10 cm for the regular resonator and 11.6 cm x 11.6 cm x 11.6 cm for the $\lambda/4.2$ -shifted resonator. To complete the resonators, we inserted and soldered one hundred copper wires, each with a radius of 0.5 mm, into the PCB cubes with a periodic spacing of $a = 1$ cm, as shown in Fig. 6a.

We equipped each resonator prototype with a 4-mm long SMA connector attached to its bottom plate for signal feeding. The SMA port functions similarly to a monopole antenna, exciting the TM modes within the resonator cavity. To characterize the electric field dis-

tribution of the TM modes, we positioned a separate monopole antenna through a pre-drilled array of holes on the top plate of each resonator, as illustrated Fig. 6b. This monopole antenna was a coaxial cable with a center conductor radius of 0.25 mm, extending 4 mm into the resonators through the holes. The hole array comprised 81 individual holes, arranged in a square grid with a period of $a = 1$ cm and a hole radius of $r_h = 3$ mm.

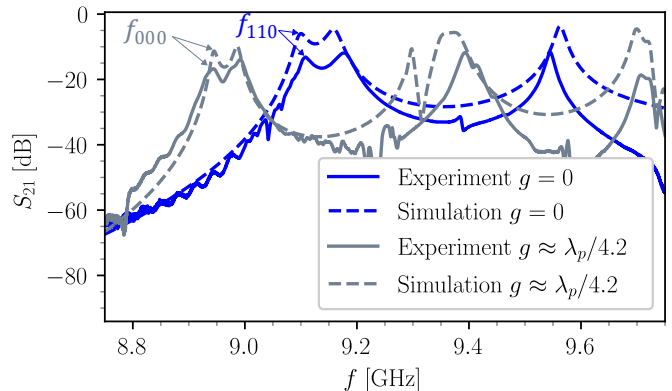


FIG. 7: Experimentally measured S_{21} parameter for WM resonators: (a) Regular resonator and (b) $\lambda_p/4.2$ -shifted resonator. Measurements were performed by placing the movable monopole antenna in the central hole. The resonance frequency of the fundamental TM mode in the regular resonator (f_{110}) is 9.11 GHz (experiment) and 9.10 GHz (simulation), while in the $\lambda_p/4.2$ -shifted resonator (f_{000}) it is 8.94 GHz (experiment and simulation).

We measured the S-parameters using a Rohde & Schwarz ZVB20 vector network analyzer (VNA) across a frequency range of 8.75-9.75 GHz. The fixed antenna on the bottom plate of each prototype was connected to one VNA port, while the movable antenna on the top plate was connected to the other port. Fig. 7 displays the measured S_{21} when the movable antenna was placed in the central hole of each prototype. We observe that the spectrum of the $\lambda_p/4.2$ -shifted resonator is red-shifted relative to that of the regular resonator, as predicted by theory for the fundamental mode. The amplitude levels and spectrum shape change slightly, suggesting that the quality factor is not significantly affected by the introduction of a $\lambda_p/4.2$ air gap.

We conducted full-wave simulations of cubic resonators, matching the experimental prototypes, using CST Studio. Copper was modeled with a conductivity of $\sigma = 5.7 \times 10^7$ S/m, while the FR-4 layers of the PCBs were represented as lossy dielectrics with a dielectric constant of $\epsilon = 4.3$ and a loss tangent of $\tan \delta = 0.025$. We measured the S_{21} parameter and positioned a field monitor at the first resonance frequency for each resonator.

We characterized the operation of the two resonators under comparison by examining the first peaks of the S_{21} -parameter spectra. These peaks correspond to the TM_{110} mode for the regular resonator and the quasi-

TM₀₀₀ mode for the $\lambda_p/4.2$ -shifted resonator, as shown in Fig. 7. Fig. 8 presents the measured electric field distributions for both prototypes at their corresponding frequencies (f_{000} for the $\lambda_p/4.2$ -shifted resonator and f_{110} for the regular one). We observe a significant improvement in field homogeneity for the $\lambda_p/4.2$ -shifted resonator. This observation is further supported by the measured form factors: 0.77 (experiment), 0.80 (simulation) for the $\lambda_p/4.2$ -shifted resonator compared to 0.61 (experiment), 0.64 (simulation) for the regular resonator.

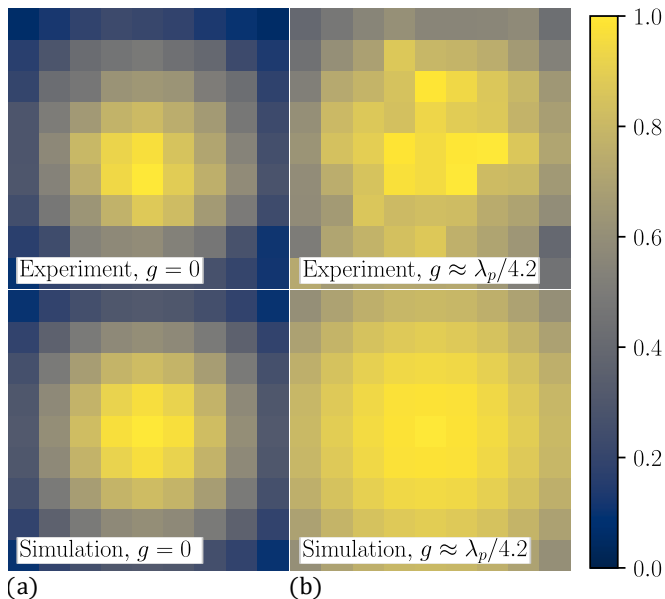


FIG. 8: Measured electric field distribution of the fundamental TM mode in wire media resonators: (a) Regular resonator and (b) $\lambda/4.2$ -shifted resonator. Pixel intensities represent the magnitude of the S_{21} parameter measured at the fundamental resonance frequencies, f_{110} and f_{000} (marked in Fig. 7), through pre-drilled holes at one end of the cavities.

Our experimental results show improved field homogeneity due to the optimized gap between the WM sample and the resonator walls. The slight discrepancies between experimental and simulation results, seen in the field maps of Fig. 8, are likely due to experimental limitations. Variations in wire length, caused by manual soldering, and potential material deformations from excessive heat may have led to wire or PCB plate bending. Additionally, the scanning procedure, where the antenna moved through holes, could have introduced slight variations if the antenna was not perfectly centered at each hole. This may explain the difficulty in pinpointing the exact location of the maximum field, which did not align precisely with the central hole as simulations predicted.

In conclusion, we introduced a method to enhance field homogeneity in WM resonators by increasing the air gap between the resonator walls and the WM sample, with the field homogeneity peaking at a gap of one-quarter of the plasma wavelength. Our theoretical model and

simulations predict a form factor of 0.92 for the effective WM model and 0.89 for the physical wire array, with the resonant mode frequency shifting toward the plasma frequency. Experimental validation was carried out with two prototype resonators: a regular WM resonator and an optimized one with a $\lambda_p/4.2$ shift. We measured the field distribution and form factor, finding significant improvements in the form factor, from 0.61 to 0.77 experimentally, and from 0.64 to 0.80 in simulations. These results validate the use of the TM₀₀₀ mode for improving the form factor in plasma haloscopes. Future work will focus on advancing cavity design, including exploring diverse cross-sections and tunable resonance frequencies.

ACKNOWLEDGEMENTS

Fermilab is operated by the Fermi Research Alliance, LLC under Contract DE-AC02-07CH11359 with the U.S. Department of Energy.

DATA AVAILABILITY STATEMENT

The data that support the findings of this study are available from the corresponding author upon reasonable request.

REFERENCES

- ¹J. Brown, “Artificial dielectrics,” *Progress in Dielectrics* **2**, 195–225 (1960).
- ²W. Rotman, “Plasma simulation by artificial dielectrics and parallel-plate media,” *IEEE Trans. Antennas Propag.* **3**, 82–95 (1962).
- ³J. B. Pendry, A. J. Holden, D. J. Robbins, and W. J. Stewart, “Low frequency plasmons in thin-wire structures,” *J. Condens. Matter Phys.* **10**, 4785 (1998).
- ⁴P. A. Belov, R. Marqués, S. I. Maslovski, I. S. Nefedov, M. Silveirinha, C. R. Simovski, and S. A. Tretyakov, “Strong spatial dispersion in wire media in the very large wavelength limit,” *Phys. Rev. B* **67**, 113103 (2003).
- ⁵E. Forati, G. W. Hanson, and D. F. Sievenpiper, “An Epsilon-Near-Zero Total-Internal-Reflection Metamaterial Antenna,” *IEEE Trans. Antennas Propag.* **63**, 1909–1916 (2015).
- ⁶C. Simovski, S. Maslovski, I. Nefedov, and S. Tretyakov, “Optimization of radiative heat transfer in hyperbolic metamaterials for thermophotovoltaic applications,” *Opt. Express* **21**, 14988–15013 (2013).
- ⁷C. Simovski, S. Maslovski, I. Nefedov, S. Kosulnikov, P. Belov, and S. Tretyakov, “Hyperlens makes thermal emission strongly super-Planckian,” *Photonics Nanostructures: Fundam. Appl.* **13**, 31–41 (2015).
- ⁸C. R. Simovski, P. A. Belov, A. V. Atrashchenko, and Y. S. Kivshar, “Wire metamaterials: physics and applications,” *Adv. Mater.* **24**, 4229–4248 (2012).
- ⁹M. S. Mirmoosa, S. Y. Kosulnikov, and C. R. Simovski, “Magnetic hyperbolic metamaterial of high-index nanowires,” *Phys. Rev. B* **94**, 075138 (2016).
- ¹⁰M. S. Mirmoosa, S. Y. Kosulnikov, and C. R. Simovski, “Double resonant wideband Purcell effect in wire metamaterials,” *J. Opt.* **18**, 095101 (2016).

- ¹¹M. Lawson, A. J. Millar, M. Pancaldi, E. Vitagliano, and F. Wilczek, “Tunable Axion Plasma Haloscopes,” *Phys. Rev. Lett.* **123**, 141802 (2019).
- ¹²A. J. Millar, S. M. Anlage, R. Balafendiev, P. Belov, K. van Bibber, J. Conrad, M. Demarteau, A. Droster, K. Dunne, A. G. Rosso, J. E. Gudmundsson, H. Jackson, G. Kaur, T. Klaesson, N. Kowitz, M. Lawson, A. Leder, A. Miyazaki, S. Morampudi, H. V. Peiris, H. S. Røising, G. Singh, D. Sun, J. H. Thomas, F. Wilczek, S. Withington, M. Wooten, J. Dilling, M. Febraro, S. Knirck, and C. Marvinney (Endorsers), “Searching for dark matter with plasma haloscopes,” *Phys. Rev. D* **107**, 055013 (2023).
- ¹³G. B. Gelmini, A. J. Millar, V. Takhistov, and E. Vitagliano, “Probing dark photons with plasma haloscopes,” *Phys. Rev. D* **102**, 043003 (2020), [arXiv:2006.06836 \[hep-ph\]](https://arxiv.org/abs/2006.06836).
- ¹⁴R. Balafendiev, C. Simovski, A. J. Millar, and P. Belov, “Wire metamaterial filled metallic resonators,” *Phys. Rev. B* **106**, 75106 (2022).
- ¹⁵J. S. Hyde, J. W. Sidabras, and R. R. Mett, “Uniform Field Resonators for EPR Spectroscopy: A Review,” *Cell Biochem. Biophys.* **77**, 3–14 (2019).
- ¹⁶R. R. Mett, W. Froncisz, and J. S. Hyde, “Axially uniform resonant cavity modes for potential use in electron paramagnetic resonance spectroscopy,” *Rev. Sci. Instrum.* **72**, 4188–4200 (2001).
- ¹⁷J. R. Anderson, R. R. Mett, and J. S. Hyde, “Cavities with axially uniform fields for use in electron paramagnetic resonance. II. Free space generalization,” *Rev. Sci. Instrum.* **73**, 3027–3037 (2002).
- ¹⁸J. S. Hyde, R. R. Mett, and J. R. Anderson, “Cavities with axially uniform fields for use in electron paramagnetic resonance. III. Re-entrant geometries,” *Rev. Sci. Instrum.* **73**, 4003–4009 (2002).
- ¹⁹L. Krauss, J. Moody, F. Wilczek, and D. E. Morris, “Calculations for cosmic axion detection,” *Phys. Rev. Lett.* **55**, 1797–1800 (1985).
- ²⁰W. U. Wuensch, S. De Panfilis-Wuensch, Y. K. Semertzidis, J. T. Rogers, A. C. Melissinos, H. J. Halama, B. E. Moskowitz, A. G. Prodell, W. B. Fowler, and F. A. Nezrick, “Results of a laboratory search for cosmic axions and other weakly coupled light particles,” *Phys. Rev. D* **40**, 3153–3167 (1989).
- ²¹R. Bradley, J. Clarke, D. Kinion, L. J. Rosenberg, K. van Bibber, S. Matsuki, M. Mück, and P. Sikivie, “Microwave cavity searches for dark-matter axions,” *Rev. Mod. Phys.* **75**, 777–817 (2003).
- ²²S. Asztalos, E. Daw, H. Peng, L. J. Rosenberg, C. Hagmann, D. Kinion, W. Stoeffl, K. van Bibber, P. Sikivie, N. S. Sullivan, D. B. Tanner, F. Nezrick, M. S. Turner, D. M. Moltz, J. Powell, M.-O. André, J. Clarke, M. Mück, and R. F. Bradley, “Large-scale microwave cavity search for dark-matter axions,” *Phys. Rev. D* **64**, 092003 (2001).
- ²³I. Stern, G. Carosi, N. Sullivan, and D. Tanner, “Avoided Mode Crossings in Cylindrical Microwave Cavities,” *Phys. Rev. Appl.* **12**, 044016 (2019).
- ²⁴T. A. Dyson, C. L. Bartram, A. Davidson, J. B. Ezekiel, L. M. Futamura, T. Liu, and C.-L. Kuo, “High-volume tunable resonator for axion searches above 7 ghz,” *Phys. Rev. Appl.* **21**, L041002 (2024).
- ²⁵C.-L. Kuo, “Large-volume centimeter-wave cavities for axion searches,” *J. Cosmol. Astropart. Phys.* **2020**, 010 (2020).
- ²⁶E. A. J. Marcatili, “Dielectric rectangular waveguide and directional coupler for integrated optics,” *Bell Syst. Tech. J.* **48**, 2071–2102 (1969).
- ²⁷A. Kumar, A. Majumder, S. Chatterjee, S. Das, and S. Kar, “A novel approach to determine the plasma frequency for wire media,” *Metamaterials* **6**, 43–50 (2012).